Semi-Nonlinear Nanophotonic Waveguides for Highly Efficient Second-Harmonic Generation

*Rui Luo, Yang He, Hanxiao Liang, Mingxiao Li, and Qiang Lin**

Quadratic optical parametric processes form the foundation for various applications related to classical and quantum frequency conversion, and have attracted significant interest recently in on-chip implementation. These processes rely on phase matching among the interacting guided modes, and refractive index engineering is a primary approach for this purpose. Unfortunately, modal phase-matching approaches developed so far only produce parametric generation with fairly low efficiencies, due to the intrinsic modal mismatch of spatial symmetries. Here, a universal design and operation principle is proposed for highly efficient optical parametric generation on integrated photonic platforms. By breaking the spatial symmetry of the optical nonlinearity of the device, nonlinear parametric interactions can be dramatically enhanced. This principle is then employed to design and fabricate a heterogeneous titanium oxide/lithium niobate nanophotonic waveguide that is able to offer second-harmonic generation with a theoretical normalized conversion efficiency as high as 2900% W^{-1} cm^{-2}, which enables the measurement of an experimental efficiency of 650% W^{-1} cm^{-2}, significantly beyond the reach of conventional modal phase-matching approaches. Unlike nonlinearity domain engineering that is material selective, the proposed operation principle can be flexibly applied to any other on-chip quadratic nonlinear platform, to support ultra-highly efficient optical parametric generation.

1. Introduction

Quadratic optical parametric processes via a $\chi^{(2)}$ nonlinearity have attracted long-lasting interest ever since the first observation of second-harmonic generation (SHG).[1,2] Their intriguing capability of creating new light through elastic photon–photon scattering forms a crucial foundation for a wide variety of applications ranging from photonic signal processing,[3,4] tunable coherent radiation,[5] frequency metrology,[6] optical microscopy,[7] to quantum information processing.[8] Recently, the development of optical parametric processes on various chip-scale platforms,[9–30] which show great promise to significantly enhance the nonlinear effects by tight confinement of optical fields, has attracted tremendous interest.

The efficiency of an optical parametric process relies essentially on phase matching among the interacting waves to sustain a coherent nonlinear interaction. To date, phase matching is dominantly realized via either domain engineering of the nonlinear susceptibility[31–33] or refractive-index engineering of the interacting optical modes.[31] Domain engineering is an efficient approach to achieve quasi-phase matching, which, however, is fairly material limited. For example, periodic poling[32–40] and orientation-patterned growth[31,41–43] are currently implemented only to ferroelectrics and III–V semiconductors, respectively. Domain engineering also has stringent requirement on the domain uniformity,[32–34] which imposes a challenge for applications that require small domain periods[28–30,33] or clean parametric noise background.[40] On the other hand, modal index engineering is able to achieve exact phase matching,[31] which can be flexibly implemented particularly to an on-chip platform that supports rich guided mode species.[9,10,12–27] Unfortunately, modal phase matching suffers from significant mode field mismatch among the interacting optical modes, which seriously degrades the nonlinear conversion efficiency.[9,10,12–27] Although periodic grating structure can be utilized to assist phase matching while maximizing mode overlap, intrinsic radiation loss is inevitably introduced.[23,44,45]

Here, we propose a universal design and operation principle of semi-nonlinear waveguides for highly efficient optical parametric generation on integrated photonic platforms. The proposed heterogeneous nanophotonic waveguides consist of a nonlinear medium exciting parametric processes and a linear medium assisting exact phase matching, which are able to combine elegantly a large nonlinearity, a strong optical confinement, and a good spatial mode match together in a single device, resulting in dramatically enhanced nonlinear parametric generation with an extremely high efficiency. To demonstrate our proposed principle, we employ a nanophotonic waveguide composed of a

R. Luo, Prof. Q. Lin
Institute of Optics
University of Rochester
Rochester, NY 14627
E-mail: qiang.lin@rochester.edu
Y. He, H. Liang, M. Li, Prof. Q. Lin
Department of Electrical and Computer Engineering
University of Rochester
Rochester, NY 14627

The ORCID identification number(s) for the author(s) of this article can be found under https://doi.org/10.1002/lpor.201800288

DOI: 10.1002/lpor.201800288

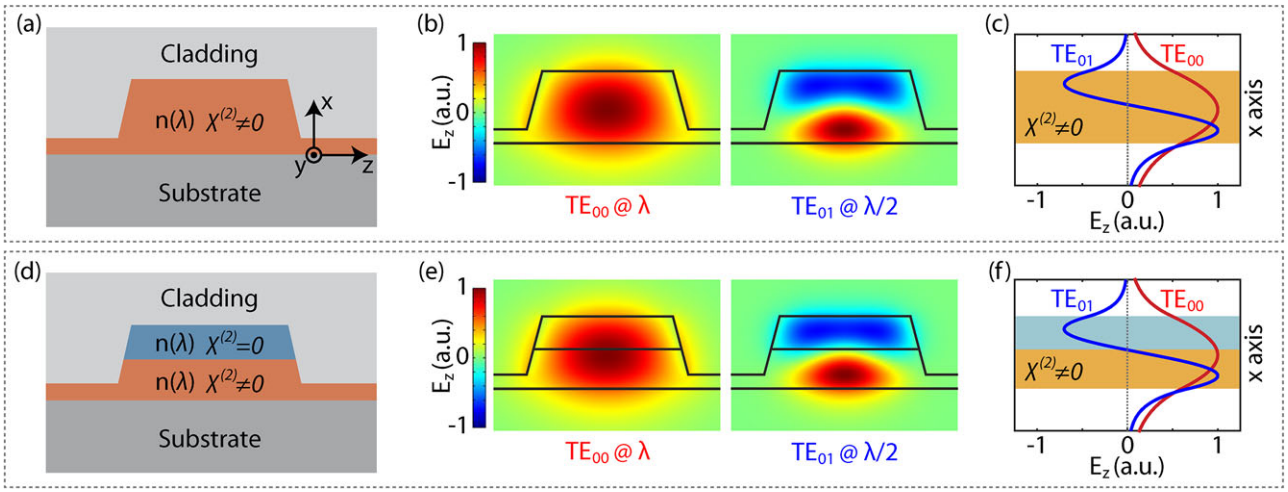

Figure 1. Illustration of the design principle of semi-nonlinear waveguides for highly efficient SHG. a) Schematic of a monolithic nanophotonic waveguide with a $\chi^{(2)}$ nonlinearity. b) Optical field (E_z) profiles of two phase-matched modes, TE_{00} at the fundamental wavelength λ and TE_{01} at the half wavelength $\lambda/2$. c) E_z as a function of the vertical position x, at the center of the waveguide, with the orange shaded area indicating the $\chi^{(2)}$ material. d) Schematic of a semi-nonlinear waveguide composed of two core materials, with both sharing the same linear refractive index $n(\lambda)$, while only the bottom layer has a non-vanished $\chi^{(2)}$ nonlinearity. e,f) counterparts of (b) and (c), respectively, for the semi-nonlinear waveguide.

highly nonlinear $\chi^{(2)}$ material, lithium niobate (LN), and a linear optical material, amorphous titanium oxide (TiO_2). The dramatically enhanced nonlinear optical interaction in the device leads to a theoretical normalized conversion efficiency as high as 2900% $W^{-1}\,cm^{-2}$ for SHG, which enables us to experimentally achieve a conversion efficiency of 36.0% W^{-1} in a waveguide only 2.35 mm long, corresponding to an experimentally recorded normalized conversion efficiency of 650% $W^{-1}\,cm^{-2}$. The proposed operation principle can be flexibly applied to any other on-chip quadratic nonlinear platform to support ultra-highly efficient optical parametric interactions, thus opening up a great avenue toward extreme nonlinear and quantum optics with great potential for broad applications in energy efficient nonlinear and quantum photonic signal processing.

2. Concept Illustration

In a quadratic nonlinear waveguide, it is well known that the phase velocities can be exactly matched among different guided modes to support a coherent nonlinear interaction.[9,10,13,16–27] When the phase-matching condition is satisfied, the efficiency of SHG (for a lossless waveguide without pump depletion) is given by the following expression[1]

$$\eta \equiv \frac{P_2}{P_1^2 L^2} = \frac{8\pi^2}{\epsilon_0 c n_1^2 n_2 \lambda^2} \frac{\zeta^2 d_{\text{eff}}^2}{A_{\text{eff}}} \tag{1}$$

where P_1 and P_2 are the powers of the input fundamental-frequency (FF) mode and the produced second-harmonic (SH) mode, respectively. L is the waveguide length, d_{eff} represents the effective nonlinear susceptibility, λ is the fundamental pump wavelength, and n_1 and n_2 are the effective refractive indices of the FF and SH modes, respectively. ϵ_0 and c are the permittivity and the speed of light, respectively, in vacuum. In Equation (1), $A_{\text{eff}} \equiv (A_1^2 A_2)^{\frac{1}{3}}$ is the effective mode area, where $A_i = \frac{(\int_{\text{all}} |\mathbf{E}_i|^2 dxdz)^3}{|\int_{\chi^{(2)}} |\mathbf{E}_i|^2 \mathbf{E}_i dxdz|^2}$, $(i = 1, 2)$, and ζ represents the spatial mode overlap factor between the FF and SH modes, given as

$$\zeta = \frac{\int_{\chi^{(2)}} (E_{1z}^*)^2 E_{2z} dxdz}{|\int_{\chi^{(2)}} |\mathbf{E}_1|^2 \mathbf{E}_1 dxdz|^{\frac{2}{3}} |\int_{\chi^{(2)}} |\mathbf{E}_2|^2 \mathbf{E}_2 dxdz|^{\frac{1}{3}}} \tag{2}$$

where $\int_{\chi^{(2)}}$ and $\int_{\text{all}}$ denote 2D integrations over the $\chi^{(2)}$ material and all space, respectively. $\mathbf{E}_1(x, z)$ and $\mathbf{E}_2(x, z)$ are the electric fields of the FF and SH modes, respectively, and E_{1z} and E_{2z} are their z-components. Here, we have assumed both of the FF and SH modes to be quasi-transverse-electric (quasi-TE) modes with electric fields dominantly lying in the device plane (e.g., see **Figure 1**a,b).

Equation (1) shows that the efficiency of SHG depends essentially on the nonlinear susceptibility, the effective mode area, and the spatial mode overlap. In particular, Equation (2) shows that the spatial mode overlap relies critically on the relative spatial symmetry between the FF and SH modes. Unfortunately, for a nonlinear waveguide, different-order guided modes generally exhibit very distinctive spatial symmetries, leading to a dramatically degraded spatial mode overlap. To illustrate this problem, we consider a nominal monolithic nanophotonic rib waveguide shown in Figure 1a, where the core material exhibits a quadratic nonlinearity. An appropriate waveguide geometry will lead to exact phase matching between the fundamental TE_{00} mode at a wavelength λ and a high-order mode (TE_{01} in our example) at the half wavelength $\lambda/2$. However, as shown in Figure 1b,c, the electric field (E_z) of the SH mode changes its polarity across the waveguide core while that of the FF mode maintains a single polarity. As a result, the nonlinear parametric interaction in the upper half of the waveguide is out of phase with that in the lower half, and therefore they cancel with each other, leading to a very small net nonlinear effect. It is exactly this modal mismatch of spatial symmetries that severely undermines the nonlinear conversion

efficiency on the majority of current nonlinear photonic chips,[9–30] although they have shown the advantage of strong mode confinement, that is, small mode areas. Consequently, a device has to rely on a long interaction length (or a high optical quality factor in the case of a resonator) to sustain the nonlinear optical process.[19]

To tackle this challenge, we propose semi-nonlinear waveguides, which leverage the fact that modal phase matching depends only on the linear properties of the waveguide independent of its nonlinearity. Therefore, by breaking the spatial symmetry of the optical nonlinearity, we shall be able to significantly enhance the strength of the nonlinear interaction. Figure 1d shows the schematic of a semi-nonlinear waveguide, which exhibits the same geometry as the monolithic waveguide shown in Figure 1a, while the top part of the core is replaced by a linear material with the same refractive index, and a vanished $\chi^{(2)}$. Since its linear refractive index profile is the same as that of the monolithic waveguide, the semi-nonlinear waveguide supports an exactly same pair of phase-matched TE_{00} mode at the FF and TE_{01} mode at the SH, with mode profiles identical to those of the monolithic waveguide (see Figure 1b,e). The thickness of the linear layer is chosen such that, for the SH mode TE_{01} with two opposite polarities, $E_z \approx 0$ at the boundary between the two core materials, resulting in a single polarity inside each of the linear and nonlinear layers. As the top linear layer does not participate in the nonlinear interaction, the parametric process only has contribution from the bottom nonlinear layer, which will not be canceled, resulting in a remarkably enhanced net nonlinear effect (which manifests as a large value of ζ in Equation (2)). The discussion above, for simplicity, has assumed an identical refractive index between the linear and nonlinear layers. In practice, the operation principle can be applied to two core materials with dissimilar refractive indices, since the semi-nonlinear waveguide offers plenty of degrees of freedom for engineering.

3. Waveguide Design

To demonstrate the proposed principle, we design a semi-nonlinear waveguide that consists of a single-crystalline LN thin-film layer as the nonlinear medium and an amorphous TiO_2 layer as the linear component. LN exhibits a large $\chi^{(2)}$ nonlinearity and a wide transparency window from ultraviolet to mid-infrared, and is an ideal medium for nonlinear parametric generation.[21–30,32–40] TiO_2 is chosen as the linear material for a few reasons. First, TiO_2 deposited by physical vapor deposition is in an amorphous phase, and the inversion symmetry leads

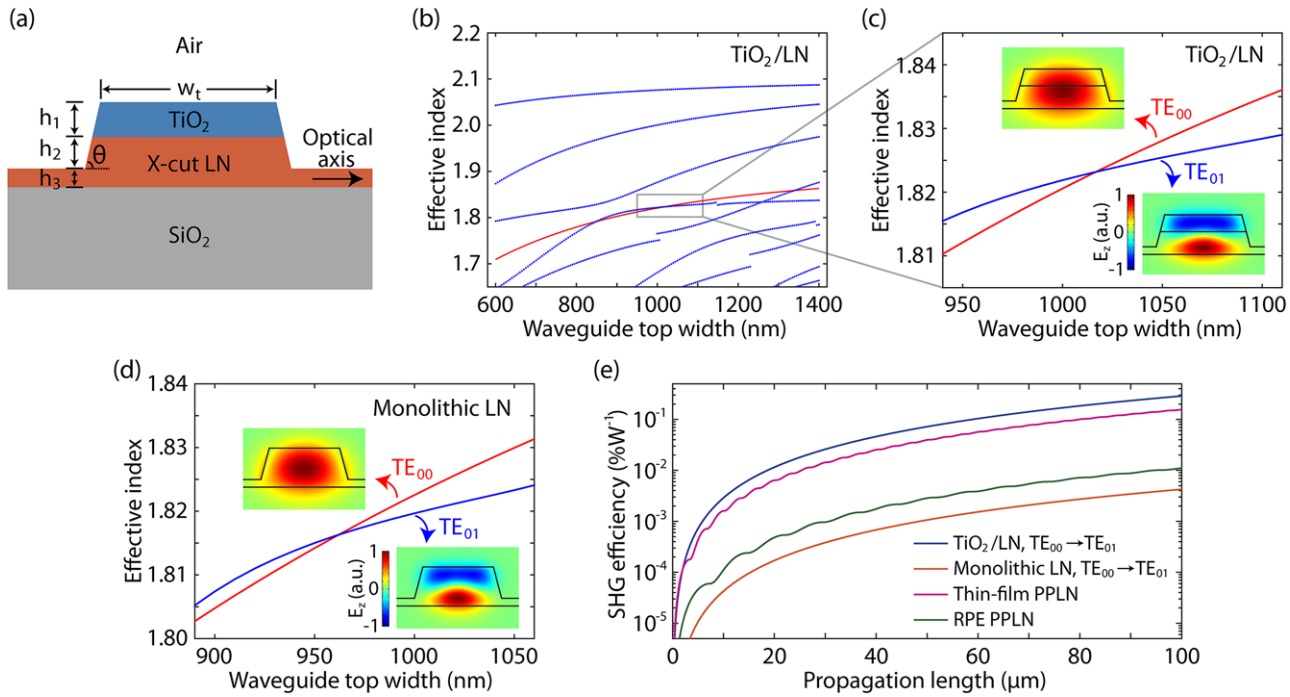

Figure 2. Design of a TiO_2/LN semi-nonlinear waveguide for an enhanced SHG efficiency. a) Schematic of the TiO_2/LN waveguide. b) Effective refractive indices of the TiO_2/LN waveguide as functions of the waveguide top width w_t, simulated by the finite element method. Other waveguide dimensions are set as $h_1 = 220$ nm, $h_2 = 200$ nm, $h_3 = 100$ nm, and $\theta = 75°$. The red curve is for the TE_{00} mode at the fundamental wavelength of 1550 nm, and the blue curves are for different quasi-TE modes at the half wavelength of 775 nm. Discontinuities in some blue curves are due to coupling with certain quasi-TM modes (not shown). c) Detailed effective indices of the TiO_2/LN waveguide as functions of w_t, showing modal phase matching between TE_{00} at 1550 nm and TE_{01} at 775 nm around $w_t = 1020$ nm. The insets show the optical field (E_z) profiles of both modes, with a shared color bar. d) Detailed effective indices as functions of w_t, for a monolithic LN waveguide, showing phase matching between TE_{00} at 1550 nm and TE_{01} at 775 nm around $w_t = 960$ nm. Other than a smaller phase-matched w_t due to different material dispersions, the geometry parameters of the monolithic LN waveguide are the same as those of the TiO_2/LN waveguide in (b) and (c), while with the TiO_2 layer replaced by LN. e) Evolution of SHG efficiencies in a TiO_2/LN semi-nonlinear waveguide, see (c), a monolithic LN waveguide, see (d), a thin-film PPLN waveguide (ref. [28]), and a typical RPE PPLN waveguide (ref. [38]), assuming no loss and no pump depletion for all types of waveguides, as well as ideally uniform poling for PPLN.

to a vanished $\chi^{(2)}$. Second, our characterization shows that an amorphous TiO_2 thin film has a relatively large refractive index of 2.137 at 1550 nm and 2.186 at 775 nm, making it suitable for strong optical confinement and flexible dispersion engineering. Third, TiO_2 also has a large bandgap and has been demonstrated for high-quality waveguides at telecom and visible wavelengths,[46–48] enabling it to be a low-loss core material that guides both FF and SH light.

The designed TiO_2/LN semi-nonlinear nanophotonic waveguide is schematically shown in **Figure 2**a. X-cut LN is employed for its large second-order nonlinearity in the device plane, ideal for efficient type-0 processes involving quasi-TE modes. Numerical simulations show that the TE_{00} mode at 1550 nm can be phase-matched to certain quasi-TE modes at 775 nm with appropriate waveguide geometries (see Figure 2b). In particular, as shown in Figure 2c, exact phase matching can be achieved between the TE_{00} mode at 1550 nm and the TE_{01} at 775 nm, the latter of which exhibits an optical mode field (see Figure 2c, insets) with two opposite polarities located separately in the linear and nonlinear core layers, a desired property we have shown in Figure 1.

Detailed simulations show that our waveguide exhibits a large overlap factor of $\zeta = 0.66$, a value significantly beyond what is achievable in monolithic nanophotonic waveguides through modal phase matching.[9,10,13,16–27] This large mode overlap factor, together with a small mode area of $A_{\text{eff}} = 2.24\ \mu m^2$ and a significant quadratic nonlinearity of $d_{\text{eff}} = d_{33} = 27\ \text{pmV}^{-1}$, enables our device to exhibit a theoretical normalized conversion efficiency as large as $\eta = 2900\%\ \text{W}^{-1}\,\text{cm}^{-2}$. In contrast, a conventional monolithic LN waveguide with a similar geometry (see Figure 2d) can only offer an efficiency of $\eta = 43\%\ \text{W}^{-1}\,\text{cm}^{-2}$, similar to other reported LN nanophotonic waveguides with modal phase matching.[23,26] This large difference directly shows the advantage of our proposed approach. Figure 2e compares evolution of the SHG efficiency as the pump light propagates in several different waveguides. It shows clearly that the η value in our semi-nonlinear waveguide is more than one order of magnitude larger than that of typical reverse-proton-exchanged (RPE) periodically poled lithium niobate (PPLN) waveguides[38] and that of monolithic LN nanophotonic waveguides,[23,26] and almost doubles that of PPLN thin films loaded with silicon nitride ridges.[28]

4. Linear Optical Properties

To confirm our simulation results, we performed device fabrication, with the LN waveguide made through a standard top-down process[24,26] and the TiO_2 layer via a lift-off approach. Details of the fabrication procedure are discussed in Appendix. **Figure 3**a shows the facet of a typical fabricated waveguide, where the TiO_2 layer landed nicely on top of the LN rib waveguide, with a geometry close to our design (see Figure 2c). Figure 3b presents the top view of the TiO_2/LN waveguide, which shows a small sidewall roughness, implying a low propagation attenuation.

The device was tested with an experimental setup schematically shown in Figure 3c. To accurately characterize the waveguide propagation loss, we fabricated microring resonators, with an example shown in Figure 3d. The microrings have a radius of 100 μm, which was chosen for a negligible bending loss. Figure 3e presents the laser-scanned transmission spectrum of such a microring, which shows clearly the TE_{00} mode family in the telecom band with a free-spectral range of 1.59 nm. Figure 3f

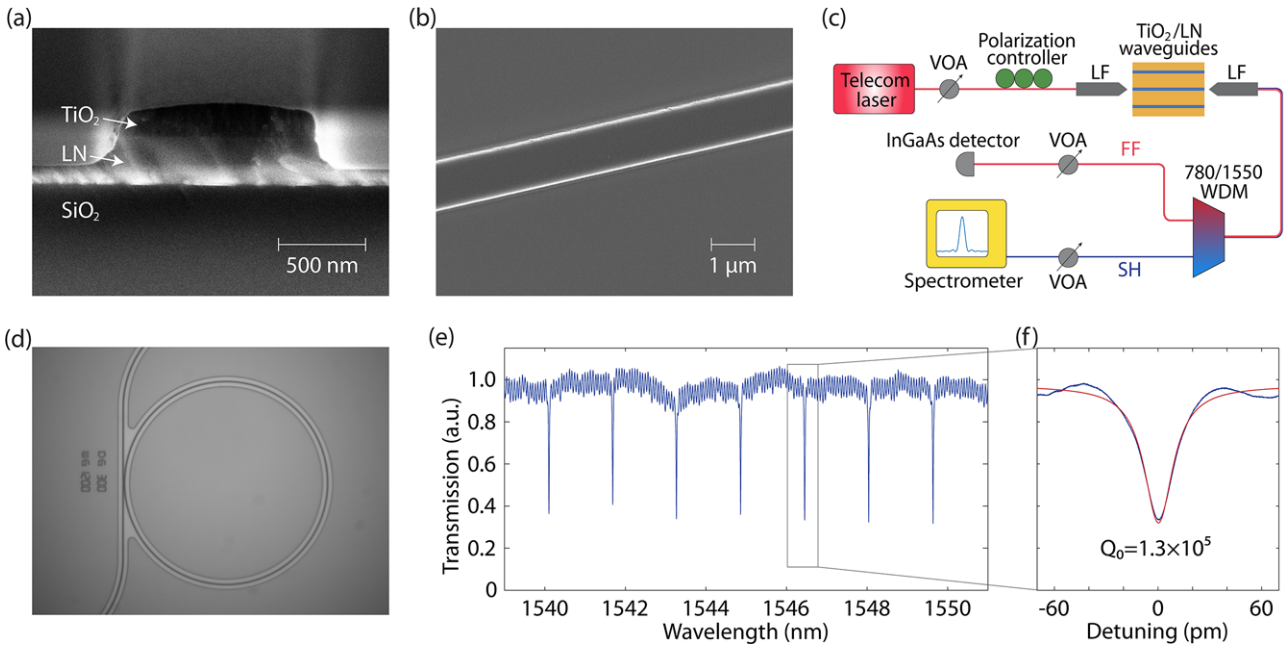

Figure 3. Characterization of fabricated devices. a) Scanning electron microscopy image of the facet of a fabricated TiO_2/LN waveguide. b) Top view of a section of the waveguide. c) Schematic of the experimental setup for device characterization and SHG measurement. VOA, variable optical attenuator; LF, lensed fiber; WDM, wavelength division multiplexer. d) Optical microscopy image of a TiO_2/LN microring resonator with a radius of 100 μm. e) Transmission spectrum of the microring resonator in the telecom band. f) Detailed transmission spectrum of a typical resonance, with experimental data shown in blue and a fitting curve shown in red.

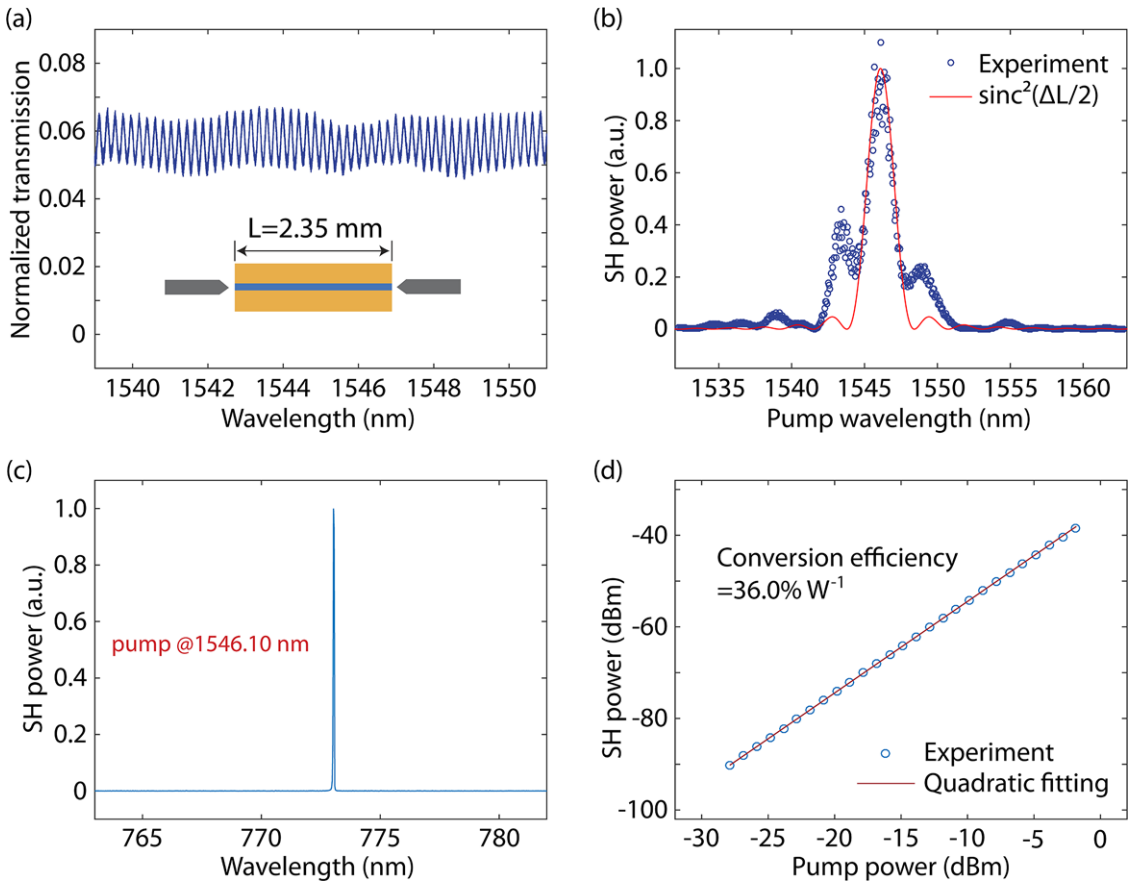

Figure 4. Measurement of SHG. a) Telecom-band transmission spectrum of the TE polarization of a TiO_2/LN straight waveguide with a length of $L = 2.35$ mm. b) Measured SHG spectrum (blue circles) of the TiO_2/LN waveguide. The red curve shows $\mathrm{sinc}^2(\Delta L/2) = [\frac{\sin(\Delta L/2)}{\Delta L/2}]^2$ for comparison, where the phase mismatch $\Delta \equiv \frac{4\pi}{\lambda}(n_2 - n_1)$. c) SHG spectrum of the device for a fixed pump wavelength of 1546.10 nm. d) Power dependence of the SHG, with experimental data shown in blue and a theoretical quadratic fitting shown in red. The theoretical fitting indicates a conversion efficiency of 36.0% W^{-1}.

presents the detailed transmission spectrum of a typical resonance, which exhibits an intrinsic quality factor of 1.3×10^5, indicating a waveguide propagation loss of 3.2 dB cm^{-1} in the telecom band.[49] For the SH mode around 775 nm, however, the current bus waveguide is very weakly coupled to the microring resonator, making it difficult to measure the quality factor in this waveband.

5. Second-Harmonic Generation

To demonstrate efficient SHG, we employed a straight waveguide with a length of about 2.35 mm, whose transmission in the telecom band is shown in **Figure 4**a for the TE polarization. From Figure 4a, we extract a fiber-to-fiber loss of 12.5 dB. Given a propagation loss of 3.2 dB cm^{-1}, we retrieve a fiber-to-chip coupling loss of 5.9 dB per facet. By scanning the pump laser wavelength, we were able to characterize the efficiency spectrum of SHG. One example is shown in Figure 4b, which indicates a phase-matched pump wavelength of about 1546 nm. The main lobe of the recorded efficiency spectrum agrees with the theoretical expectation from the sinc^2-function. The strong side lobes are likely introduced by slight non-uniformity of the waveguide (e.g., potential thickness variations of the core layers).

By fixing the pump wavelength at 1546.10 nm where the peak conversion is located, we observed coherent radiation from its SH at 773.05 nm, shown as a sharp peak in Figure 4c. The measured SH power shows a quadratic dependence on the pump power (see Figure 4d), which agrees very well with the theoretical expectation. Fitting the experimental data, we obtained an on-chip conversion efficiency of 36.0% W^{-1} (see Figure 4d), indicating an experimentally recorded normalized conversion efficiency of 650% $W^{-1}cm^{-2}$. This value is about a fourfold increase compared with the previous record of SHG in LN in the same waveband.[28,39]

The measured conversion efficiency is lower than the simulation result $\eta L^2 (= 160\%\ W^{-1})$, due to a few reasons. The first reason lies in the propagation losses of the waveguide. We have measured a propagation loss of 3.2 dB cm^{-1} for the FF mode. As a rough estimate, we assume that of the SH mode to be ≈12.8 dB cm^{-1}, since the propagation loss is dominated by Rayleigh scattering from the roughness of the waveguide surface, which scales with wavelength as $1/\lambda^2$.[50] Consequently, the theoretical conversion efficiency is estimated to be ≈96.0% W^{-1}

for the 2.35-mm-long waveguide, after we take into account the propagation losses. Meanwhile, the coupling loss of the SH carried in a high-order waveguide mode is fairly underestimated, resulting from the large mode mismatch between the waveguide and the receiving lensed fiber, leading to a conservative estimation of the measured conversion efficiency. In addition, the slight waveguide non-uniformity could also impact the conversion efficiency to a certain extent.

All the above technical issues can be addressed with further optimization. On the one hand, unlike grating-assisted waveguides,[23,44,45] the scattering loss in our waveguide with translational symmetry is not physically fundamental, and can be mitigated by optimized fabrication. For example, chemical-mechanical polishing can be employed to increase the surface smoothness, as well as the waveguide uniformity.[25] On the other hand, a single-mode on-chip coupler can be utilized to minimize the facet coupling loss, especially at the SH.[19] Therefore, we expect the measured conversion efficiency can be increased considerably in the near future.

6. Conclusion and Discussion

In conclusion, we have proposed and demonstrated a universal design and operation principle for quadratic parametric processes on integrated photonic platforms, which is able to achieve modal phase matching with a large nonlinearity, a small mode area, and a large mode overlap factor for extremely efficient SHG. With this principle, we designed a TiO_2/LN semi-nonlinear waveguide that is able to offer a theoretical conversion efficiency as high as 2900% W^{-1} cm^{-2}, more than one order of magnitude higher than those achievable in RPE PPLN and monolithic on-chip LN waveguides.[23,26,38] The designed geometry enabled us to record an SHG efficiency of 36.0% W^{-1} inside a waveguide only 2.35 mm long, corresponding to a normalized efficiency of 650% W^{-1} cm^{-2}.

The normalized conversion efficiency of our device is comparable with those of recently reported on-chip PPLN waveguides.[28,30] However, our demonstrated approach is free from the complicated periodic poling process. Domain engineering has been regarded as the holy grail for quadratic nonlinear photonics,[31–33] which, however, is material selective. Our proposed approach, instead, can be universally applied to any on-chip quadratic nonlinear platforms, including, for example, certain dielectrics,[9,10] group IV,[11,12] III–V,[17,19,20] and II–VI[31] semiconductor chips to which domain engineering is challenging to apply. Therefore, our proposed approach may open up a great avenue toward extreme nonlinear and quantum optics with ultra-high nonlinear conversion efficiencies that are promising for broad applications in energy efficient nonlinear and quantum photonic signal processing.

On the other hand, as shown in Figure 1, the proposed semi-nonlinear nanophotonic waveguide intriguingly separates the waveguide into a nonlinear part that experiences a nonlinear conversion gain and a linear part that experiences only a linear propagation loss, which forms a natural parity-time-symmetric system that is of great potential for non-Hermitian photonic applications.[51,52]

Appendix

A.1. Device Fabrication

We started from a LN-on-insulator wafer by NANOLN, with 300 nm of X-cut LN sitting on 2-μm-thick buried oxide and a silicon substrate. LN waveguides were patterned by electron-beam lithography (EBL), with ZEP520A as the resist. After etching LN waveguides with ion milling, we removed residual resist with oxygen plasma followed by diluted hydrofluoric acid. Then, in order to pattern the TiO_2 layer on top of the etched LN waveguides, we employed aligned EBL, after which we used physical vapor deposition to deposit TiO_2. Next, we soaked the wafer in 1165 resist remover, which removed the resist, leaving us the heterogeneous TiO_2/LN waveguides. Finally, the device chip was hand-cleaved for light coupling into the waveguides.

A.2. Experimental Setup

Pump light from a continuous-wave tunable telecom-band laser was coupled into the device chip through a lensed fiber. At the waveguide output, the FF pump light was collected together with the SH light by a second lensed fiber. Then, light at the two wavebands was separated by a 780/1550 WDM, after which the FF light was directed to an InGaAs detector for characterization, while the SH light was sent to a spectrometer for detection. A fiber polarization controller was used to achieve optimal coupling of the wanted polarization, and VOAs were employed to study the power dependence of SHG.

Acknowledgements

The authors thank Chengyu Liu at Cornell University for helpful discussions on fabrication of TiO_2. This work was supported in part by the National Science Foundation under Grant No. ECCS-1641099, ECCS-1509749 and ECCS-1810169, by the Defense Threat Reduction Agency under Grant No. HDTRA11810047, and by the Defense Advanced Research Projects Agency SCOUT program through Grant No. W31P4Q-15-1-0007 from the U.S. Army Aviation and Missile Research, Development, and Engineering Center (AMRDEC). The project or effort depicted was or is sponsored by the Department of the Defense, Defense Threat Reduction Agency. The content of the information does not necessarily reflect the position or the policy of the federal government, and no official endorsement should be inferred. This work was performed in part at the Cornell NanoScale Science & Technology Facility (CNF), a member of the National Nanotechnology Coordinated Infrastructure (NNCI), which is supported by the National Science Foundation (Grant No. NNCI-1542081), and at the Cornell Center for Materials Research (National Science Foundation, DMR-1719875).

Conflict of Interest

The authors declare no conflict of interest.

Keywords

integrated photonics, lithium niobate, nonlinear optics, optical parametric generation

Received: October 30, 2018
Revised: December 12, 2018
Published online: January 11, 2019

[1] R. W. Boyd, *Nonlinear Optics*, 3rd ed., Academic Press, San Diego, CA, **2008**.
[2] N. Bloembergen, *IEEE J. Sel. Top. Quantum Electron.* **2000**, *6*, 876.
[3] C. Langrock, S. Kumar, J. E. McGeehan, A. E. Willner, M. M. Fejer, *J. Lightwave Technol.* **2006**, *24*, 2579.
[4] A. E. Willner, S. Khaleghi, M. R. Chitgarha, O. F. Yilmaz, *J. Lightwave Technol.* **2014**, *32*, 660.
[5] M. H. Dunn, M. Ebrahimzadeh, *Science* **1999**, *286*, 1513.
[6] S. T. Cundiff, J. Ye, *Rev. Mod. Phys.* **2003**, *75*, 325.
[7] P. J. Campagnola, C. Y. Dong, *Laser Photonics Rev.* **2011**, *5*, 13.
[8] J. W. Pan, Z. B. Chen, C. Y. Lu, H. Weinfurter, A. Zeilinger, M. Żukowski, *Rev. Mod. Phys.* **2012**, *84*, 777.
[9] J. S. Levy, M. A. Foster, A. L. Gaeta, M. Lipson, *Opt. Express* **2011**, *19*, 11415.
[10] A. Billat, D. Grassani, M. H. Pfeiffer, S. Kharitonov, T. J. Kippenberg, C. S. Brès, *Nat. Commun.* **2017**, *8*, 1016.
[11] M. Cazzanelli, F. Bianco, E. Borga, G. Pucker, M. Ghulinyan, E. Degoli, E. Luppi, V. Véniard, S. Ossicini, D. Modotto, S. Wabnitz, R. Pierobon, L. Pavesi, *Nat. Mater.* **2012**, *11*, 148.
[12] S. Yamada, B. S. Song, S. Jeon, J. Upham, Y. Tanaka, T. Asano, S. Noda, *Opt. Lett.* **2014**, *39*, 1768.
[13] D. P. Lake, M. Mitchell, H. Jayakumar, L. F. dos Santos, D. Curic, P. E. Barclay, *Appl. Phys. Lett.* **2016**, *108*, 031109.
[14] K. Rivoire, Z. Lin, F. Hatami, W. T. Masselink, J. Vučković, *Opt. Express* **2009**, *17*, 22609.
[15] S. Buckley, M. Radulaski, J. L. Zhang, J. Petykiewicz, K. Biermann, J. Vučković, *Opt. Lett.* **2014**, *39*, 5673.
[16] M. Savanier, A. Andronico, A. Lemaître, E. Galopin, C. Manquest, I. Favero, S. Ducci, G. Leo, *Opt. Lett.* **2011**, *36*, 2955.
[17] C. Xiong, W. Pernice, K. K. Ryu, C. Schuck, K. Y. Fong, T. Palacios, H. X. Tang, *Opt. Express* **2011**, *19*, 10462.
[18] P. S. Kuo, J. Bravo-Abad, G. S. Solomon, *Nat. Commun.* **2014**, *5*, 3109.
[19] X. Guo, C. L. Zou, H. X. Tang, *Optica* **2016**, *3*, 1126.
[20] L. Chang, A. Boes, X. Guo, D. T. Spencer, M. Kennedy, J. D. Peters, N. Volet, J. Chiles, A. Kowligy, N. Nader, D. D. Hickstein, E. J. Stanton, S. A. Diddams, S. B. Papp, J. E. Bowers, *Laser Photonics Rev.* **2018**, *12*, 1800149.
[21] R. Geiss, S. Saravi, A. Sergeyev, S. Diziain, F. Setzpfandt, F. Schrempel, R. Grange, E. B. Kley, A. Tünnermann, T. Pertsch, *Opt. Lett.* **2015**, *40*, 2715.
[22] J. Lin, Y. Xu, J. Ni, M. Wang, Z. Fang, L. Qiao, W. Fang, Y. Cheng, *Phys. Rev. Appl.* **2016**, *6*, 014002.
[23] C. Wang, X. Xiong, N. Andrade, V. Venkataraman, X. F. Ren, G. C. Guo, M. Lončar, *Opt. Express* **2017**, *25*, 6963.
[24] R. Luo, H. Jiang, S. Rogers, H. Liang, Y. He, Q. Lin, *Opt. Express* **2017**, *25*, 24531.
[25] R. Wolf, I. Breunig, H. Zappe, K. Buse, *Opt. Express* **2017**, *25*, 29927.
[26] R. Luo, Y. He, H. Liang, M. Li, Q. Lin, *Optica* **2018**, *5*, 1006.
[27] L. Wang, C. Wang, J. Wang, F. Bo, M. Zhang, Q. Gong, M. Lončar, Y. F. Xiao, *Opt. Lett.* **2018**, *43*, 2917.
[28] L. Chang, Y. Li, N. Volet, L. Wang, J. Peters, J. E. Bowers, *Optica* **2016**, *3*, 531.
[29] A. Rao, M. Malinowski, A. Honardoost, J. R. Talukder, P. Rabiei, P. Delfyett, S. Fathpour, *Opt. Express* **2016**, *24*, 29941.
[30] C. Wang, C. Langrock, A. Marandi, M. Jankowski, M. Zhang, B. Desiatov, M. M. Fejer, M. Lončar, *Optica* **2018**, *5*, 1438.
[31] A. S. Helmy, P. Abolghasem, J. Stewart Aitchison, B. J. Bijlani, J. Han, B. M. Holmes, D. C. Hutchings, U. Younis, S. J. Wagner, *Laser Photonics Rev.* **2011**, *5*, 272.
[32] D. S. Hum, M. M. Fejer, *C. R. Physique* **2007**, *8*, 180.
[33] V. Y. Shur, A. Akhmatkhanov, I. Baturin, *Appl. Phys. Rev.* **2015**, *2*, 040604.
[34] M. M. Fejer, G. Magel, D. H. Jundt, R. L. Byer, *IEEE J. Quantum Electron.* **1992**, *28*, 2631.
[35] M. Yamada, N. Nada, M. Saitoh, K. Watanabe, *Appl. Phys. Lett.* **1993**, *62*, 435.
[36] L. E. Myers, R. Eckardt, M. Fejer, R. Byer, W. Bosenberg, J. Pierce, *J. Opt. Soc. Am. B* **1995**, *12*, 2102.
[37] K. Mizuuchi, H. Ohta, K. Yamamoto, M. Kato, *Opt. Lett.* **1997**, *22*, 1217.
[38] K. R. Parameswaran, J. R. Kurz, R. V. Roussev, M. M. Fejer, *Opt. Lett.* **2002**, *27*, 43.
[39] K. R. Parameswaran, R. K. Route, J. R. Kurz, R. V. Roussev, M. M. Fejer, M. Fujimura, *Opt. Lett.* **2002**, *27*, 179.
[40] J. S. Pelc, C. Langrock, Q. Zhang, M. M. Fejer, *Opt. Lett.* **2010**, *35*, 2804.
[41] S. Yoo, R. Bhat, C. Caneau, M. Koza, *Appl. Phys. Lett.* **1995**, *66*, 3410.
[42] L. Eyres, P. Tourreau, T. Pinguet, C. Ebert, J. Harris, M. Fejer, L. Becouarn, B. Gerard, E. Lallier, *Appl. Phys. Lett.* **2001**, *79*, 904.
[43] V. Tassev, M. Snure, R. Peterson, K. Schepler, R. Bedford, M. Mann, S. Vangala, W. Goodhue, A. Lin, J. Harris, M. Fejer, P. Schunemann, in *Nonlinear Frequency Generation and Conversion: Materials, Devices, and Applications XII*, Vol. *8604*, SPIE **2013**, p. 86040V.
[44] S. Somekh, A. Yariv, *Appl. Phys. Lett.* **1972**, *21*, 140.
[45] A. Rao, J. Chiles, S. Khan, S. Toroghi, M. Malinowski, G. F. Camacho-González, S. Fathpour, *Appl. Phys. Lett.* **2017**, *110*, 111109.
[46] S. S. Djordjevic, K. Shang, B. Guan, S. T. Cheung, L. Liao, J. Basak, H. F. Liu, S. Yoo, *Opt. Express* **2013**, *21*, 13958.
[47] B. Guha, J. Cardenas, M. Lipson, *Opt. Express* **2013**, *21*, 26557.
[48] C. C. Evans, C. Liu, J. Suntivich, *Opt. Express* **2015**, *23*, 11160.
[49] P. Rabiei, W. H. Steier, C. Zhang, L. R. Dalton, *J. Light. Technol.* **2002**, *20*, 1968.
[50] P. K. Tien, *Appl. Opt.* **1971**, *10*, 2395.
[51] L. Feng, R. El-Ganainy, L. Ge, *Nat. Photonics* **2017**, *11*, 752.
[52] R. El-Ganainy, K. G. Makris, M. Khajavikhan, Z. H. Musslimani, S. Rotter, D. N. Christodoulides, *Nat. Phys.* **2018**, *14*, 11.